COBEM 2021 26th International Congress of Mechanical Engineering
ABCM Associação Brasileira de Engenharia e Ciências Mecânicas
November 22-26, 2021, Virtual Congress, Brazil

COB-2021-0068
DYNAMICS OF A ROTOR WITH GEOMETRIC NON-LINEARITY

Luis Fernando dos Anjos
Rodrigo Nicoletti
Universidade de São Paulo, Escola de Engenharia de São Carlos, Avenida Trabalhador São Carlense 400, São Carlos, SP, Brasil
luis.anjos@usp.br
rnicolet@sc.usp.br

Abstract. *Rotating machines are usually modeled and analyzed by the finite element method. In such analyses, a linear behavior of the system is observed due to the linear nature of the modeling method. However, depending on the geometry of the rotor and on the level of external loading, nonlinear effects can appear, and the conventional finite element model is no longer appropriated (it cannot predict the nonlinear effects in the system). In this work, we study the nonlinear behavior of rotors with geometric non-linearity. The geometric non-linearity appears when large lateral displacements are imposed to the rotor. Due to the boundary constraints (restrictions imposed by the bearings), such large lateral displacements result in an axial loading, which increases the stiffness of the rotor (stiffening effect). In this work, we model a flexible rotor by the finite element method and we include in the model an additional stiffness matrix related to the geometric stiffening effect. The unbalance response of the system is analyzed for different levels of unbalance. The results show a clear bending of the resonance peak towards higher frequencies (stiffening effect) and, for higher levels of unbalance, the jump effect (sudden decrease or increase of vibration amplitude as we increase or decrease the rotating speed). We also show that hydrodynamic bearings tend to attenuate the nonlinear effects caused by the geometric non-linearity in comparison to the case using ball bearings.*

Keywords: *Rotordynamics, Finite Element Method, Centrifugally Stiffened Beam, Nonlinear Dynamics*

1. INTRODUCTION

Rotating Machines are largely present in society and their applications cover a wide range of sectors, such as agriculture, mining, large industries and household products. The knowledge of the dynamic and vibratory behavior of these machines is fundamental for the production system, because it is possible to take due precautions to guarantee engineering design. By knowing the range of usable frequencies, the vibration modes of the rotor, and some others characteristics, it is possible to provide more safety, comfort and economy for the manufacturers and for the end users of these machines (Nicoletti, 2013).

Commonly, rotating systems are mathematically modeled using the Finite Element Method (FEM) due to the difficulty of analytically modeling such systems. With this method, one can know the response of a rotor both in the time and in the frequency domains (Nelson and McVaugh, 1976; Nelson, 1980). However, the classic FEM does not consider the non-linear effects on the system and, as these effects can significantly change a system's response, some results may be very different from reality (Strogatz, 1994).

There are several ways in which non-linear phenomena can occur in a dynamic system (Fonseca *et al.*, 2016; Mignolet *et al.*, 2013). One of them is the presence of axial efforts in the structure due to large transverse displacements, which increases the stiffness of the rotor. A spring system whose assembly results in the appearance of forces which is not coincident with the line of action may produce non-linear effects (Fig. 1a). Furthermore, beams that have different thicknesses, e.g. sudden changes in cross section along the beam's length, are also subject to them (Fig. 1b).

Similar nonlinear behavior is observed on shafts (Łuczko, 2002) with different diameters and, in this case, the non-linear effects are increased by unbalance forces. The considerable importance of studying non-linear rotors is mainly because that the behavior of a non-linear system can be very different from a linear one. Examples of typical non-linear phenomena in dynamic systems are: bifurcation (response appearing at more than one frequency for a single, fixed excitation frequency), stiffening (changes in resonance frequency due to changes in excitation frequency), jump (sudden change of response amplitude after the natural frequency), among others.

In literature, most of the works focus on the non-linearity caused by the bearings (Wu *et al.*, 2011), by the seals (Shen *et al.*, 2008), by rubbing (Cao *et al.*, 2011), and by cracking (Cao *et al.*, 2013). However, the non-linearity can also be caused by the shaft geometry itself. Slender rotors tend to present nonlinear effects like stiffening (Shad *et al.*, 2012), jump phenomenon (Yuan *et al.*, 2014), bifurcation (Guido and Adiletta, 1999), and nonlinear modes (Yabuno *et al.*, 2011).

The first studies on the nonlinear effects caused by the rotor geometry focused on de Laval rotors with long and thin

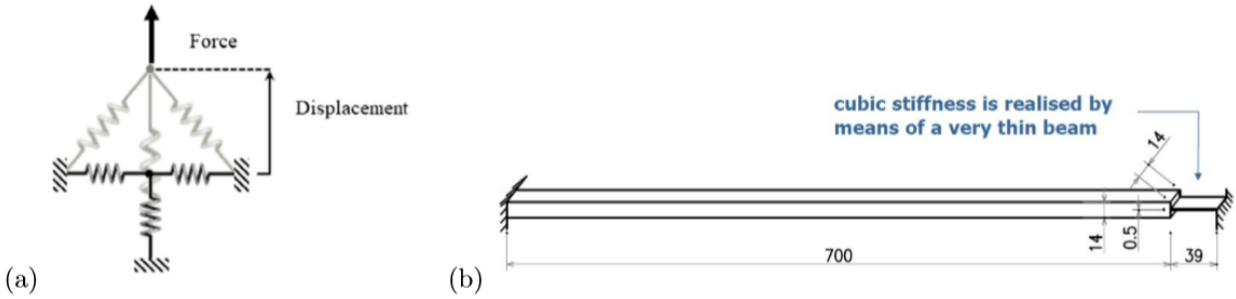

Figure 1. Structures subject to non-linear effects: a) linear system of springs (Gatti *et al.*, 2019), b) beam with different cross sections (Golinval, 2017).

shafts (Adiletta *et al.*, 1996; Guido and Adiletta, 1999). Such configuration can present nonlinear restoring forces under high amplitude vibration conditions (Shad *et al.*, 2012), or when subjected to gravity, which bows horizontal rotors and it results in non-symmetric restoring forces (Yabuno *et al.*, 2011). If the cross-section of the shaft is not circular, it is also possible to observe nonlinear effects like bifurcation (Yu *et al.*, 2018). More recently, focus has been done on the dynamics of bolted-joint rotors (Yuan *et al.*, 2014; Li *et al.*, 2019; Wang *et al.*, 2021). In this case, the shaft is composed of two sections connected by a bolted flange, and it can present sub-synchronous vibration and bifurcation. The dynamics of dual-rotors has also been studied in literature, where stiffening effects and jump phenomenon can also be observed (Liu *et al.*, 2020).

As we can see, the effect of the geometry on the nonlinear behavior of rotors has been studied in literature with main focus on slender rotors or combined rotors (bolted-joint and dual). However, the effect of cross-section variations of the shaft in the overall dynamics of the rotor, and consequent nonlinear effect, has not been investigated yet. In this work, a numerical simulation of a stepped shaft (Fig. 2) with geometric non-linearity (presenting one and two disks) are studied using the Finite Element Method for some different conditions. In order to take account non-linear effects, it was included in the FEM model an additional stiffness matrix related to the geometric stiffening effect, that varies in time and frequency (Gavin, 2012).

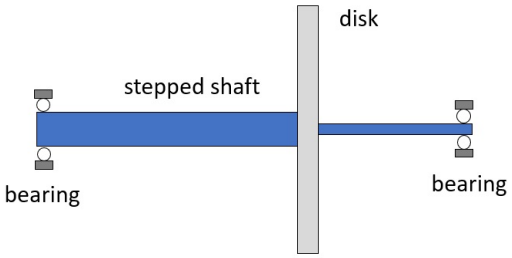

Figure 2. Stepped shaft under study.

2. MATHEMATICAL MODEL OF THE NON-LINEAR ROTOR

2.1 The Equations of Motion

It is well known that the dynamic equation of a rotor-bearing system modeled by the FEM can be formulated as follows:

$$\boldsymbol{M}\ddot{\boldsymbol{q}} + (\boldsymbol{D} - \Omega\boldsymbol{G})\dot{\boldsymbol{q}} + \boldsymbol{K}\boldsymbol{q} = \boldsymbol{f} \tag{1}$$

where Ω is the angular speed of the rotor, $\boldsymbol{q}$ is the nodal displacement vector, $\boldsymbol{f}$ is the unbalance force vector, $\boldsymbol{M}$ is the global inertia matrix, $\boldsymbol{D}$ is the global damping matrix, $\boldsymbol{G}$, is the global gyroscopic matrix, and $\boldsymbol{K}$ is the global stiffness matrix (Nelson and McVaugh, 1976). In this work, it was assumed that the unbalance caused by the shaft was not relevant compared to the unbalance of the disk, so the force vector can be calculated by:

$$\boldsymbol{f} = \left\{ \begin{array}{ccccccccc} 0 & \cdots & 0 & 0 & m_d e\Omega^2 \cos\Omega t & m_d e\Omega^2 \sin\Omega t & 0 & \cdots & 0 \end{array} \right\}^T \tag{2}$$

where the non-zero terms of the force vector refer to the degrees-of-freedom of lateral displacements of the disk. The term m_d refers to the mass of the disk and e refers to the eccentricity (distance between the geometric center and the gravity center).

The matrices in eq. (1), with the exception of the global damping matrix $\boldsymbol{D}$, can be obtained through FEM using Euler-Bernoulli theory when the shaft is long and thin (that is the case of this work). In this case, the governing equation is linear, as none of the matrices depends on the displacement vector. In order to consider non-linear effects, it is necessary to make a modification to the classic model, by adding a geometric stiffness matrix. The purpose of this matrix is to connect the transverse displacement of the rotor with an increase in stiffness caused by internal axial loads. Thus, the bigger the displacement is, the bigger the influence of geometric stiffness matrix becomes, resulting in a completely different effect in relation to the linear case. The equation for calculating this matrix, which is called geometric stiffness matrix (Gavin, 2012), is:

$$\boldsymbol{K_g} = \frac{T}{L}\begin{bmatrix} \frac{6}{5} & 0 & 0 & \frac{L}{10} & \frac{-6}{5} & 0 & 0 & \frac{L}{10} \\ & \frac{6}{5} & \frac{L}{10} & 0 & 0 & \frac{-6}{5} & \frac{L}{10} & 0 \\ & & \frac{2L^2}{15} & 0 & 0 & \frac{-L}{10} & \frac{-L^2}{10} & 0 \\ & & & \frac{2L^2}{15} & \frac{-L}{10} & 0 & 0 & \frac{-L^2}{30} \\ & & & & \frac{6}{5} & 0 & 0 & \frac{L}{10} \\ & & & & & \frac{6}{5} & \frac{-L}{10} & 0 \\ & & sym. & & & & \frac{-L^2}{15} & 0 \\ & & & & & & & \frac{-L^2}{15} \end{bmatrix} \tag{3}$$

where T is the axial force present on the shaft finite element, and L is the length of the element.

When a given finite element presents nodal displacements, the final length of the element depends on the displacement of the node $i+1$ regarding the node i, in both orthogonal directions:

$$L_d = \sqrt{(y_{i+1} - y_i)^2 + (z_{i+1} - z_i)^2 + L^2} \tag{4}$$

Therefore, the axial strain in the element is:

$$\epsilon_x = \frac{L_d - L}{L} \tag{5}$$

which results in the axial force T:

$$T = \frac{E\epsilon_x}{A} \tag{6}$$

In the equations above, L_d represents the deformed length of the shaft element, ϵ_x is the axial strain of the element, E is the material Young modulus, and A is the cross-section area of the element.

Hence, the complete governing equation of the rotor considering the non-linear stiffening effect caused by transverse deformation is given by:

$$\boldsymbol{M}\ddot{\boldsymbol{q}} + (\boldsymbol{D} - \Omega\boldsymbol{G})\dot{\boldsymbol{q}} + (\boldsymbol{K} + \boldsymbol{K_g})\boldsymbol{q} = \boldsymbol{f} \tag{7}$$

This equation represents a system of second-order ordinary differential equations. The length of the nodal displacement vector, and hence the number of equations in the system, depends on the number of nodes, and consequently degrees-of-freedom, used in the finite element model. In terms of the dynamics of the system, a system with n degrees-of-freedom allows the calculation of n natural frequencies of the rotor. But, in most engineering cases, only a few natural

frequencies (usually the lowest ones) are important because the speed range on a rotating machine does not reach very high frequencies. Thus, in order to reduce the computational cost, a modal reduction of the equation was used, removing the terms corresponding to the higher frequencies.

For the modal transformation, it is necessary to solve the eigenvalue problem of eq. (7), in the linear, static and undamped case (i.e without the terms that multiply $\dot{\boldsymbol{q}}$ and without the $\boldsymbol{K_g}$ matrix). By doing this, it is possible to obtain the modal matrix $\boldsymbol{\Phi_{n,n}}$, which corresponds to the eigenvectors associated to all the natural frequencies of the system. If the modal matrix is normalized by mass, the normal modes appear in ascending order of natural frequencies, so the first column of the matrix is related to the normal mode associated with the first natural frequency, and so on. Then, taking only the first m natural frequencies and normal modes, the transformation of the physical coordinates into modal coordinates is be as follows:

$$\boldsymbol{q_n} = \boldsymbol{\Phi_{n,m}\eta_m} \tag{8}$$

Hence, the governing equation in modal coordinates can be expressed as:

$$\overline{\boldsymbol{M}}\ddot{\boldsymbol{\eta}} + (\overline{\boldsymbol{D}} - \Omega\overline{\boldsymbol{G}})\dot{\boldsymbol{\eta}} + (\overline{\boldsymbol{K}} + \boldsymbol{K_g})\boldsymbol{\eta} = \overline{\mathrm{f}} \tag{9}$$

where:

$$\overline{\boldsymbol{M}} = \boldsymbol{\Phi^t}_{\boldsymbol{m,n}}\boldsymbol{M\Phi_{n,m}} \tag{10}$$

$$\overline{\boldsymbol{G}} = \boldsymbol{\Phi^t}_{\boldsymbol{m,n}}\boldsymbol{G\Phi_{n,m}} \tag{11}$$

$$\overline{\boldsymbol{K}} = \boldsymbol{\Phi^t}_{\boldsymbol{m,n}}\boldsymbol{K\Phi_{n,m}} \tag{12}$$

$$\overline{\boldsymbol{K_g}} = \boldsymbol{\Phi^t}_{\boldsymbol{m,n}}\boldsymbol{K_g\Phi_{n,m}} \tag{13}$$

$$\overline{\boldsymbol{f}} = \boldsymbol{\Phi^t}_{\boldsymbol{m,n}}\boldsymbol{f} \tag{14}$$

The system of equation in eq. (9) presents order $m < n$.

Matrix $\overline{\boldsymbol{D}}$ is given by a diagonal matrix whose coefficients are related to the damping factor of the normal mode. In this work, all normal modes have the same damping factor, set to 4%. Hence:

$$\overline{\boldsymbol{D}}_{\boldsymbol{i,j}} = \begin{cases} 2\zeta\omega_i, & i = j \\ 0, & i \neq j \end{cases} \tag{15}$$

where ζ is the damping factor, and ω_i is the i^{th} natural frequency in ascending order.

After integrating eq. (9) and obtaining the vector of nodal coordinates $\boldsymbol{\eta}(t)$, it is possible to return to the physical coordinates $\boldsymbol{q}(t)$ by applying eq. (8).

2.2 The Rotor Model

For modeling the rotor with FEM, it was necessary to subdivide the domain of the problem into a finite number of sub-domains represented by nodes and elements. Each node has a group of degrees-of-freedom (DOF) that keeps the movement only in specified directions. In this work, the finite element has two nodes with four DOFs in each node,

corresponding to: translation in y-axis, translation in z-axis, rotation in y-axis ($\beta = -\frac{\partial z}{\partial x}$), and rotation in z-axis ($\gamma = \frac{\partial y}{\partial x}$), where the x-axis is in the axial direction of the rotor.

The shaft was divided into 9 nodes (8 elements), so that the system had 36 DOF before the application of the boundary conditions. Most of the found frequencies have values far above the typical frequencies of rotating machines, so only the first and second natural frequencies of the rotor were analyzed. The disk was considered rigid with lumped parameters (mass and inertia) and it was positioned at a single node of the model. The bearings allow rotating motion of the shaft, and they can present damping. Both bearings are located at the shaft extremities.

The system is study is a steel shaft with two different cross-sections: the first part of the shaft has a diameter of 10 mm of diameter and a length of 400 mm, whereas the second part of the shaft has a diameter of 4 mm and a length of 100 mm. Considering this shaft geometry, we studied three different operating conditions:

- **Condition 1 (one disk):** An 8 mm thick steel disk with a radius of 50 mm is positioned in the region where the diameter of the shaft changes. The unbalance mass, corresponding to the disk mass, is 0.493 kg. The assembly characteristics of the shaft is shown in Figure 3. Ball bearings are mounted at the ends of the shaft, whose stiffness values are presented in Table 1. Bearing #1 represents a simply-supported condition of the rotor, whereas Bearing #4 represents a fully constrained condition of the rotor. Bearings #2 and #3 represent intermediate conditions between simply-supported and fully constrained. The damping is considered negligible in all cases.

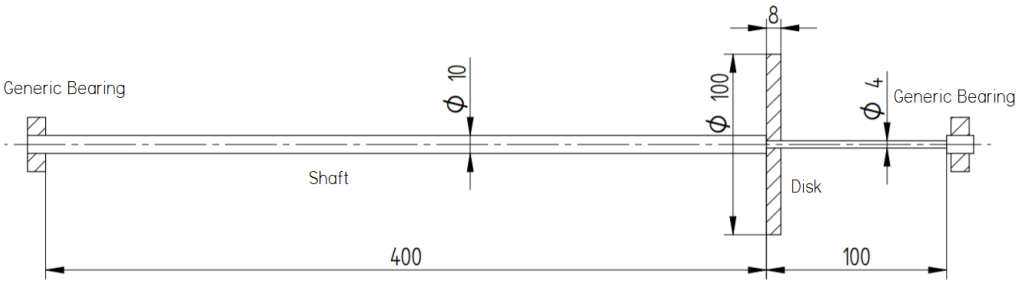

Figure 3. Representation of the rotor system with one disk.

Table 1. Stiffness values for the ball bearings in Conditions 1 and 2.

Bearing number	$\mathbf{k_{yy}(N/m)}$	$\mathbf{k_{zz}(N/m)}$	$\mathbf{k_{\beta\beta}(N.m)}$	$\mathbf{k_{\gamma\gamma}(N.m)}$
1	inf	inf	0	0
2	inf	inf	57,4	57,4
3	inf	inf	313	313
4	inf	inf	10^6	10^6

- **Condition 2 (two disks):** In this case, we add a second disk, with the same physical characteristics of the first, so that there are two identical unbalance forces in the system. The second disk is positioned in the center of the region with the largest diameter of the shaft, as shown in Figure 4. The bearings used in the simulations are the same as those in the first condition.

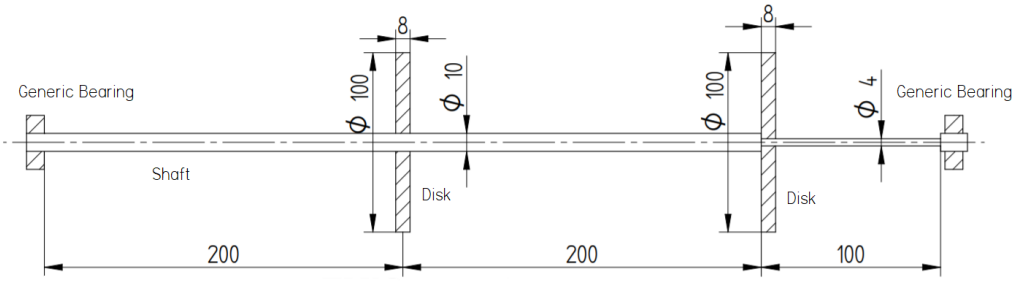

Figure 4. Representation of the rotor system with two disks.

- **Condition 3 (hydrodynamic bearings):** In this case, we adopt the rotor of the first condition, represented in Figure 3, with hydrodynamic bearings instead of rolling bearings. For the simulation, we modeled the hydrodynamic

bearings by their equivalent dynamic coefficient (linearized bearings), so that the only non-linearity in the system comes from the rotor geometry. For this, a cylindrical bearing, with L:D ratio equal to 1 and two axial grooves is used. The values of stiffness and damping coefficients of these bearings are provided by Someya (1989), which depend on the rotating speed of the rotor and on other properties of the bearing (Sommerfeld number). Figure 5 shows the stiffness and damping coefficients adopted in the numerical simulations as a function of the rotating frequency. The properties of the adopted hydrodynamic bearings are presented in Table 2.

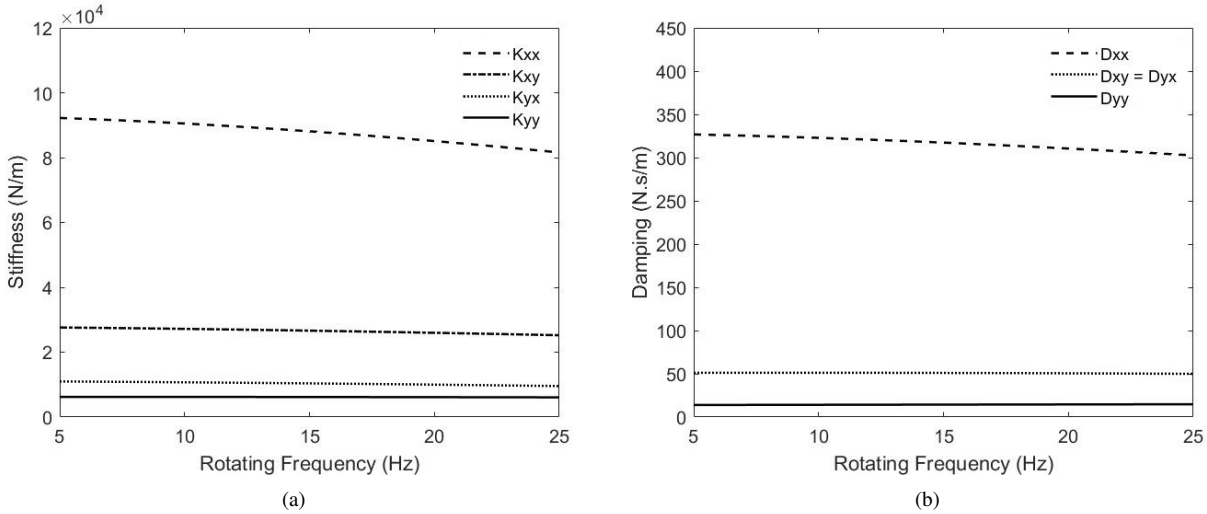

(a) (b)

Figure 5. Coefficients of the hydrodynamic bearing as a function of the rotating frequency: a) stiffness, b) damping.

Table 2. Properties of the hydrodynamic bearings in Condition 3.

property	*value*	*unit*
Bearing diameter	10.1	mm
Rotor diameter at the bearing	10.0	mm
Bearing clearance	0.05	mm
Oil dynamic viscosity	0.032	Pa.s
Load on the first bearing (left)	4.925	N
Load on the second bearing (right)	2.429	N

2.3 Numerical Simulation

All the numerical simulations were performed in MATLAB environment. The frequency response graphics were produced through sequential calculations, using numerical integration (4th order Runge Kutta method) for a defined frequency. Hence, to obtain a complete graphic, the frequency was changed by steps of 0.1 Hz and the unbalance response was obtained.

In order to calculate the non-linear effects in the system, the geometric stiffness matrix had to be updated at every step in time of the program, because its values depend on the deformation of the rotor. Also, to visualize the difference of the responses during run-up and run-down, the values of the rotating frequency was increased to a maximum value and then decreased to zero. Moreover, the initial condition for the problem at a given frequency was the steady-state solution of the previous frequency. As the values of the geometric stiffness matrix are different comparing frequency $n-1$ with frequency $n+1$ (initial conditions for calculating the solution at frequency n, in run-up and run-down, respectively), at some moments, it can be noticed this difference in behavior between the two solutions.

3. NUMERICAL RESULTS

We adopted four different unbalance eccentricities for each simulation condition. Figure 6 presents the unbalance response results for Condition #1. We can clearly see in Figure 6 the nonlinear effects in the resonance peak, as the unbalance increases. As the unbalance increases, the resonance peak tends to higher frequencies, this resulting in a "bending" effect of the peak towards higher frequencies. Such effect is a result of the *stiffening* of the rotor as larger lateral displacements take place near the critical speed, thus increasing the axial load in the rotor and, consequently, increasing the geometric stiffness.

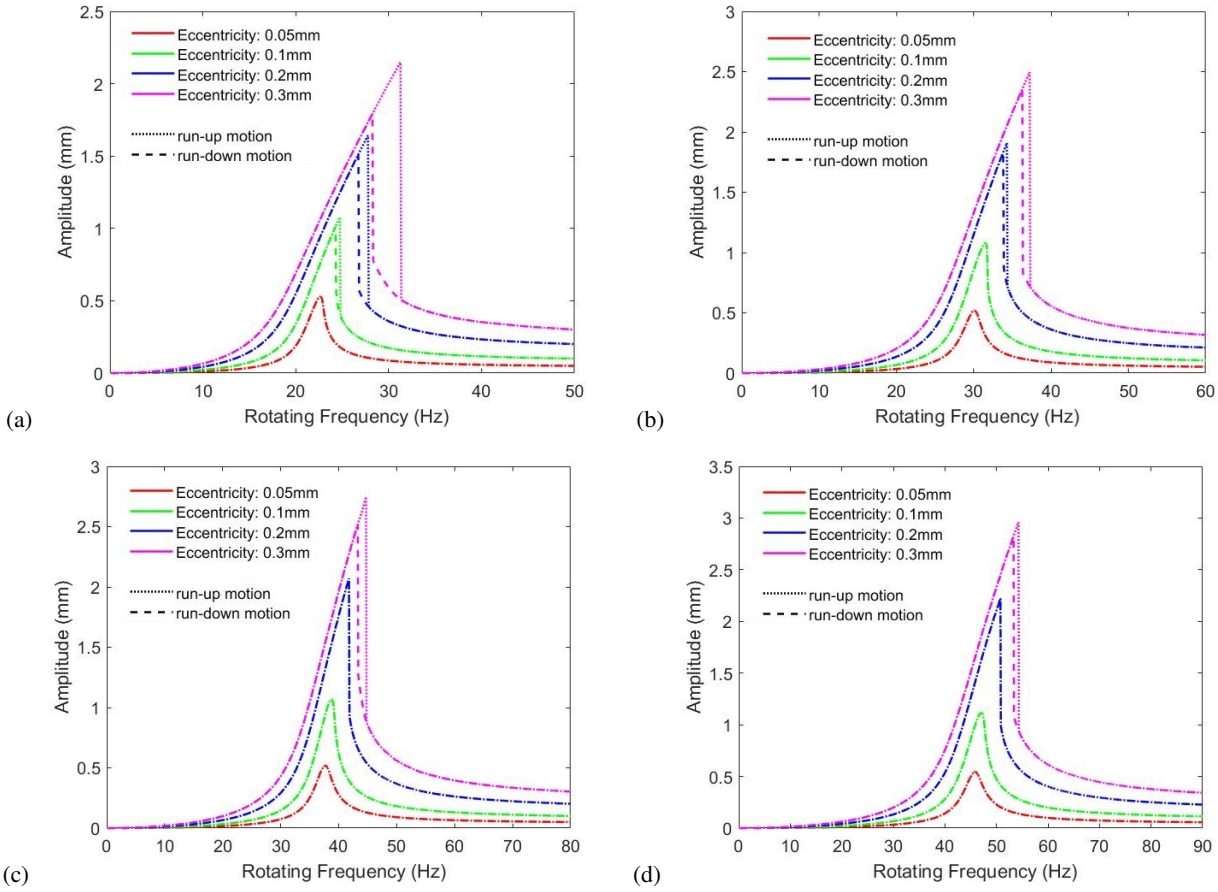

Figure 6. Unbalance response of the rotor with four different ball bearings under Condition #1: a) bearing number 1, b) bearing number 2, c) bearing number 3, d) bearing number 4.

In addition, we observe a sudden change in the vibration amplitude of the rotor as we pass through the critical speed, which is an evidence of another nonlinear effect: the *jump phenomenon*. Such phenomenon occurs both in run-up and run-down operating conditions, and they are more evident under higher unbalance conditions. Furthermore, the increase in resonance amplitude does not proportionally follow the increase in unbalance force. That is another clear nonlinear effect observed in the results: the *nonlinear relationship* between input force and output vibratory response.

Considering the four boundary conditions in use, the simply-supported case presented the highest nonlinear behavior, as seen in the Figure 6a. A possible explanation for this result is the fact that lower values of stiffness in the bearings allow greater freedom of movement of the rotor, which can facilitate nonlinear responses. Consequently, more rigid bearings resulted in lower response amplitude of the rotor, for the same eccentricity and unbalance force. However, the rotor presented higher resonance peaks with bearings with higher stiffness. This means that the nonlinear behavior of a system can be beneficial in some circumstances, such as reducing the resonance peak amplitude (Gatti *et al.*, 2019).

The frequency response for Condition #2 can be seen in Figure 7. The fact that there are two disk in the system leads to the presence of two resonance peaks for this condition. Both peaks presented nonlinear effects very similar to those seen in Figure 6. Again, the system containing the bearings with lower stiffness presented a more accentuated nonlinear behavior. Smaller resonance peaks are also observed in the response of the system with lower stiffness.

Finally, we present the results of the system under Condition #3, with hydrodynamic bearings. The unbalance response for this condition is shown in Figure 8a for four different unbalance eccentricities. Compared to the results obtained in Conditions #1 and #2, the rotating system with hydrodynamic bearings showed few nonlinear characteristics. In fact, the only observed nonlinear behavior was the stiffening effect at the second resonance, as shown in Figure 8b .

Thus, we can see that hydrodynamic bearings can attenuate the nonlinear effects caused by the geometric non linearity, due to their inherent higher damping in comparison to rolling bearings. However, the results obtained may be different from the experimental ones, since the nonlinear effects associated with fluid of the hydrodynamic bearings were neglected (we adopted linearized equivalent dynamic coefficients for the bearings).

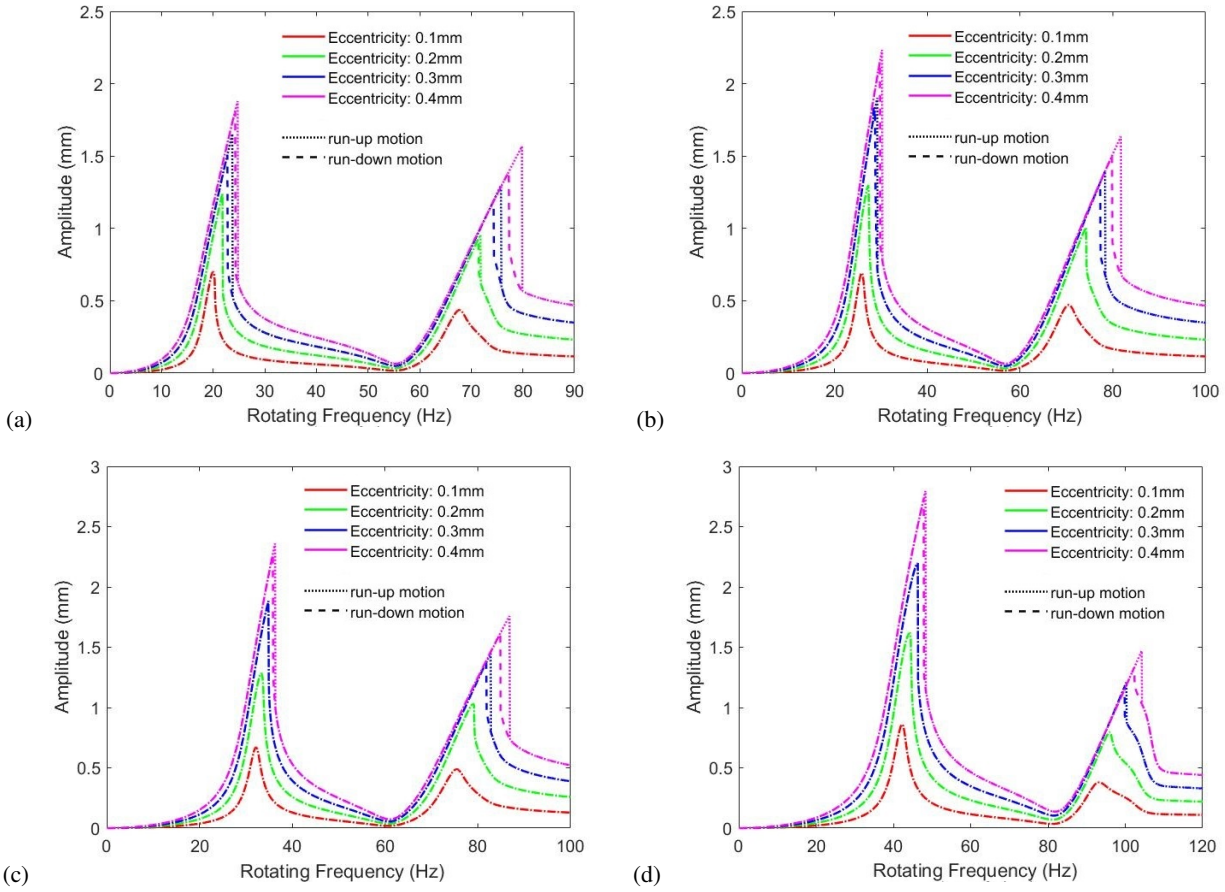

Figure 7. Unbalance response of the rotor with four different ball bearings under Condition #2: a) bearing number 1, b) bearing number 2, c) bearing number 3, d) bearing number 4.

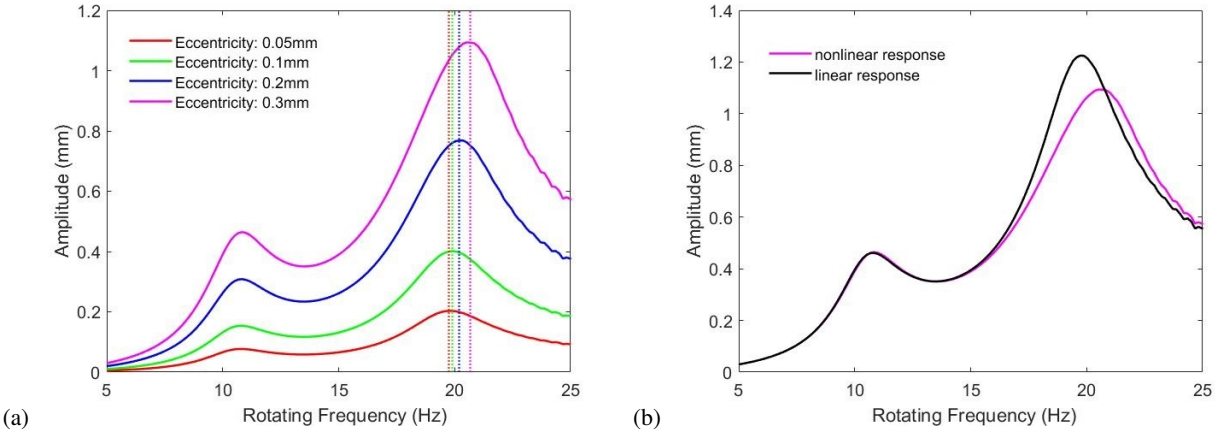

Figure 8. Unbalance response of the rotor under Condition #3: a) different eccentricities, b) comparison between linear and nonlinear response for the same eccentricity of 0.3 mm.

4. CONCLUSION

In this work, the dynamic behavior of a rotor with geometric non linearity was studied using the Finite Element Method with a complementary matrix that adds the nonlinear effects. The rotating system in study consisted of a shaft with two different diameters (10 mm and 4 mm), whose geometry presented a sudden change between these two sections. The first studied operating condition had ball bearings positioned at the ends of the shaft and a disk positioned where the sudden change of diameter occurs in the shaft; the second studied operating condition considered the same rotating system of

the first condition with a second disk placed in the center of the region with the largest diameter; and the third studied operating condition had the same configuration as the first one, but with hydrodynamic bearings.

The unbalance response obtained in all conditions showed a typical nonlinear behavior and this behavior increased significantly with increasing unbalance forces. The systems analyzed in the first and in the second operating conditions exhibited a clear stiffening effect, i.e. the resonance peak "bent" towards higher frequencies. As a consequence, the jump phenomenon was clearly observed in the results. That was more evident by comparing the results during run-up and run-down.

Regarding the third studied operating condition (rotor with hydrodynamic bearings), the obtained results showed that the nonlinear effects were attenuated. This attenuation was caused by the inherent higher damping of the hydrodynamic bearings in comparison to rolling bearings. However, it was still possible to observe the "bending" of the resonance peak due to the stiffening of the rotor caused by the geometric non linearity.

5. ACKNOWLEDGMENTS

This project was supported by FAPESP (Fundação de Amparo à Pesquisa do Estado de São Paulo), under Grant no. 2019/12455-9 and Grant no. 2021/00327-6, and CNPq (Conselho Nacional de Desenvolvimento Científico e Tecnológico), under Grant no. 301118/2018-3.

6. REFERENCES

Adiletta, G., Guido, A.R. and Rossi, C., 1996. "Nonperiodic motions of a jeffcott with nonlinear elastic restoring forces". *Nonlinear Dynamics*, Vol. 11, p. 37–59.

Cao, J.Y., Ma, C.B., Ziang, Z.D. and Liu, S.G., 2011. "Nonlinear dynamic analysis of fractional order rub-impact rotor system". *Communications in Nonlinear Science and Numerical Simulation*, Vol. 16, No. 3, pp. 1443–1463.

Cao, J.Y., Xue, S.M., Lin, J. and Chen, Y.Q., 2013. "Nonlinear dynamic analysis of a cracked rotor-bearing system with fractional order damping". *Journal of Computation and Nonlinear Dynamics*, Vol. 8, No. 3, p. 031008.

Fonseca, C.A., Aguiar, R.R. and Weber, H.I., 2016. "On the non-linear behaviour and orbit patterns of rotor/stator contact with a non-conventional containment bearing". *International Journal of Mechanical Sciences*, Vol. 105, pp. 117–125.

Gatti, G., Brennan, M. and Tang, B., 2019. "Some diverse examples of exploiting the beneficial effects of geometric stffness nonlinearity". *Mechanical Systems and Signal Processing*, Vol. 120, No. 1, pp. 4–20.

Gavin, H.P., 2012. *Geometric stiffness effect in 2d and 3d frames*. tech. rep., Duke University, Durham.

Golinval, J.C., 2017. *On the use of principal component analysis for parameter identification and damage detection in structures*. (Ericeira), p. Keynote 1, ICEDyn 2017 INT. CONF. ON STRUCTURAL ENGINEERING DYNAMIC.

Guido, A.R. and Adiletta, G., 1999. "Dynamics of a rigid unbalanced rotor with nonlinear elastic restoring forces. part i: Theoretical analysis". *Nonlinear Dynamics*, Vol. 19, pp. 359–385.

Li, Y., Luo, Z., Liu, Z. and Hou, X., 2019. "Nonlinear dynamic behaviors of a bolted joint rotor system supported by ball bearings". *Archive of Applied Mechanics*, Vol. 89.

Liu, J., Wang, C. and Luo, Z., 2020. "Research nonlinear vibrations of a dual-rotor system with nonlinear restoring forces". *Journal of the Brazilian Society of Mechanical Sciences and Engineering*, Vol. 42, p. 461.

Łuczko, J., 2002. "A geometrically non-linear model of rotating shafts with internal resonance and self-excited vibration". *Journal of sound and vibration*, Vol. 255, No. 3, pp. 433–456.

Mignolet, M.P., Przekop, A., Rizzi, S.A. and Spottswood, S.M., 2013. "A review of indirect/nonintrusive reduced order modeling of nonlinear geometric structures". *Journal of Sound and Vibration*, Vol. 332, No. 10, pp. 2437–2460.

Nelson, H.D., 1980. "A finite rotating shaft element using timoshenko beam theory". *Journal of Mechanical Design*, Vol. 102, No. 4, pp. 793–803.

Nelson, H.D. and McVaugh, J.M., 1976. "The dynamics of rotor-bearing systems using finite element". *Journal of Engineering for Industry*, Vol. 98, No. 2, pp. 593–600.

Nicoletti, R., 2013. *Estudo do controle ativo e passivo de vibrações em sistemas rotativos e estruturais*. Universidade de São Paulo, Escola de Engenharia de São Carlos, São Carlos.

Shad, M.R., Michon, G. and Berlioz, A., 2012. "Nonlinear dynamics of rotors due to large deformations and shear effects". *Applied Mechanics and Materials*, Vol. 110-116, pp. 3593–3599.

Shen, X.Y., Jia, J.H., Zhao, M. and Jing, J.P., 2008. "Experimental and numerical analysis of nonlinear dynamics of rotor-bearing-seal system". *Nonlinear Dynamics*, Vol. 53, No. 1-2, pp. 31–44.

Someya, T., 1989. *Journal-bearing databook*. Springer, Berlim, 1st edition.

Strogatz, S.H., 1994. *Nonlinear dynamics and chaos*. Perseus Books, New York, 2nd edition.

Wang, L., Wang, A., Jin, M., Yin, Y., Heng, X. and Ma, P., 2021. "Nonlinear dynamic response and stability of a rod fastening rotor with internal damping effect". *Archive of Applied Mechanics*, Vol. 91, p. 3851–3867.

Wu, X.C., Lin, B., Liu, F. and Han, X.S., 2011. "Review of non-linear rotor-bearing dynamics system". *Advances in Engineering Design and Optimization*, Vol. 37-38, pp. 1130–1137.

Yabuno, H., Kashimura, T., Inoue, T. and Ishida, Y., 2011. "Nonlinear normal modes and primary resonance of horizontally supported jeffcott rotor". *Nonlinear Dynamics*, Vol. 66, pp. 377–387.

Yu, T.J., Zhou, S., Yang, X.D. and Zhang, W., 2018. "Global dynamics of a flexible asymmetrical rotor". *Nonlinear Dynamics*, Vol. 91, pp. 1041–1060.

Yuan, Q., Gao, J. and Li, P., 2014. "Nonlinear dynamics of the rod-fastened jeffcott rotor". *Journal of Vibration and Acoustics*, Vol. 136, p. 021011.

7. RESPONSIBILITY NOTICE

The authors are solely responsible for the printed material included in this paper.